GEORG-AUGUST-UNIVERSITÄT
GÖTTINGEN

Fakultät für
Physik

Bachelor's Thesis

Hemmung von Peptidaggregation

Inhibition of peptide aggregation

prepared by

Julian Tim Brennecke

from Hildesheim

at the Max-Planck-Institute for Biophysical Chemistry

Thesis period:	22nd October 2012 until 28th January 2013
First Rreferee:	Prof. Dr. Bert de Groot
Second referee:	Prof. Dr. Helmut Grubmüller

Abstract

In the presented study short sequences of the Aβ peptide where simulated. Aβ oligomers are known to be the main reason for Alzheimer's disease. Therefore, not only simulations with the ^{16}KLVFFAE^{22} and the ^{30}AIIGLM^{35} Aβ fragments, known to aggregate from *in vitro* studies, are carried out, but also ligands known to inhibit aggregation are simulated. The results show that one of the ligands prevents beta-sheet formation which is a critical step for fibril formation, via competition for hydrogen bonds. In addition coulomb interactions are found to play a major role in ligand-peptide interaction.

Contents

Nomenclature

Abbreviations

Abbreviation	Meaning
Amber FF	Amber ff99SB*-ILDN force field
APP	Amyloid Precursor Protein
Charmm FF	Charmm36 force field
FAD	familial Alzheimer's disease
FF	Force Field
MD	Molecular Dynamics
NMR	Nuclear Magnetic Resonance
pbc	periodic boundary conditions
PME	Particle Mash Ewald
VdW	Van der Waals force

1. Theoretical background

1.1. Introduction

From *in vivo* studies it is known that protein aggregates are related to many diseases (e.g. Alzheimer's disease)[1]. There are also many *in vitro* studies that show the toxicity of oligomeric aggregates[2]. Unfortunately, the majority of experimental studies can not reveal driving forces on a molecular level. Therefore, MD simulations are applied that give us the opportunity to learn more about critical motions and underlying forces in proteins. Knowledge of these forces can also help in drug development. If one is capable of investigating forces that drive aggregation and the way existing drugs hinder aggregation, it might be possible to develop highly effective drugs.

1.2. The Aβ peptide

The Aβ peptide is related to Alzheimer's disease (AD) *in vivo*[3]. Therefore it is of interest to carry out research on the aggregation behaviour of this peptide.

1.2.1. Formation and structure

In vivo the Aβ peptide is derived from the Amyloid precursor protein (APP)[4]. APP itself maps to chromosome 21[5], a reason for increased occurrence of Alzheimer's Disease (AD) in down syndrome (trisomy 21) patients[6]. The APP is cleaved by either the α-secretase or the β-secretase[7]. This process yields different intermediate products, both further processed by γ-secretase[8]. The cleavage product of APP by β-secretase and γ-secretase is the Aβ peptide that consists of 39-43 amino acids[9]. Mutations on APP are found to increase Aβ production *in vivo*[10]. In order to come up with therapeutic strategies for e.g. AD, it is important to know about the role of Aβ in humans. However, little is known about the actual role of

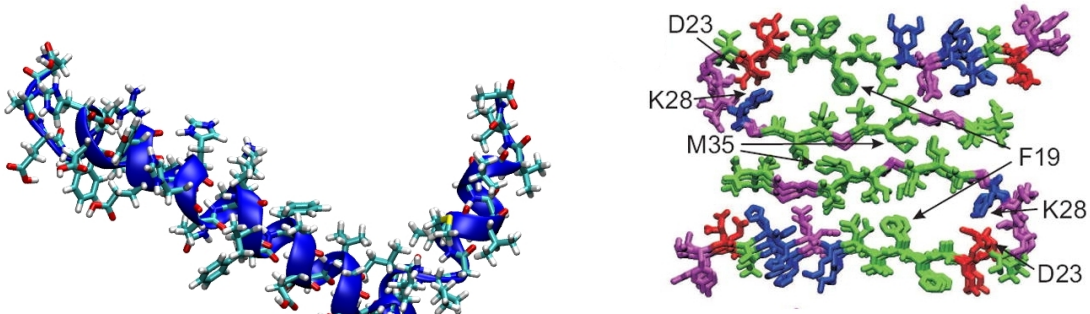

(a) Structure of soluble Aβ_{1-42} resolved by NMR (PDB ID 1IYT)[13].

(b) Model of Aβ_{1-40} in an aggregated state. Based on solid-state NMR with additional constraints from electron microscopy[14].

Figure 1.1.: Misfolding of the Aβ peptide is suggested to lead to conversion from the natural helical structure to a beta-sheet aggregated state.

this particular peptide. Recent studies showed that it has antimicrobial function[11]. Other studies provided evidence for a role in neuronal transfer[12].

In the natural state the Aβ peptide consists of two helices linked via a beta-turn[13]. It is proposed that misfolding might lead to the exposure of regions that are known to form aggregates[1]. It was demonstrated that different sequences in the Aβ_{1-42} can form aggregates on their own, leading to polymorphic structures[15]. A common motif along these polymorphic structures is the dry steric zipper interface between the peptides[15]. This means that the peptides form a beta-sheet that excludes the solvent from its inner interface. Resolved full length Aβ structures show that parts of the peptide are found in these interfaces (see figure 1.1b). As many of these structures stack together, amyloid fibrils are formed. Their inner part consist of a highly organized beta-sheet stack called amyloid spine or backbone. This motif was found for the different types of amyloid state related diseases[16].

It is mandatory for MD studies to concentrate on smaller systems, known to behave like the full length system as suitable model systems. This reduces computational efforts and therefore provides the chance to get access to larger timescales of simulation. As it is known from former studies that a variety of short sequences of the Aβ peptide form aggregates on their own[15, 17] and that they can also be inhibited[18] it is of particular interest to focus on them. In the presented study the focus is on ^{16}KLVFFAE^{22} and on ^{30}AIIGLM^{35}.

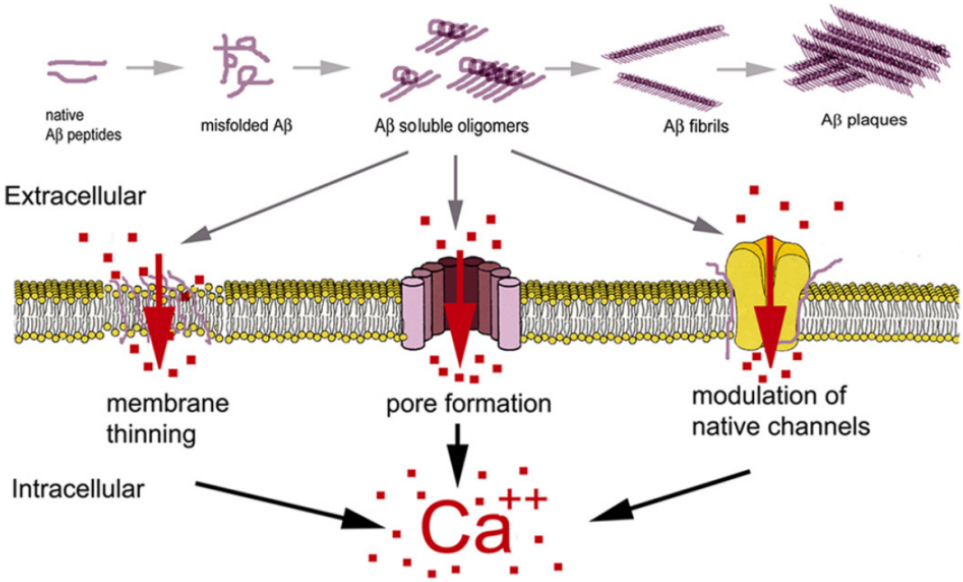

Figure 1.2.: Mechanisms of toxicity proposed for oligomeric aggregates of the Aβ-peptide [19]

1.2.2. Mechanisms of toxicity

The suggested mechanisms of toxicity of the Aβ peptide involve the oligomeric state as a key player[20]. Neither full size plaques nor monomers play an essential role in toxicity[21]. It was found that $A\beta_{1-42}$ seems to be the more toxic form because it is more prone to undergo aggregation[22]. This becomes especially evident from familial types of Alzheimer's disease (FAD) in which increased $A\beta_{1-42}$ production is found[23]. Other studies demonstrate that the $A\beta_{1-42}$ to $A\beta_{1-40}$ ratio is crucial[24]. The importance of this ratio is also indicated by studies looking at the correlation between AD and down syndrome[25].
Three different mechanisms of toxicity have been proposed (see figure 1.2). Interactions between the oligomers and the membrane lead to membrane thinning[26, 27]. The membrane peptide interaction may also lead to cation selective pore formation[28]. In addition, Aβ oligomers are able to interact with already existing Ca^{2+} channels[29]. All of these changes in the membrane lead to disruption of the membrane integrity and therefore to cell death.

1.2.3. Therapeutic strategies

As AD gets more abundant in the aging society, it is not astonishing that a drug to cure AD is one of the most urgently pursued goals of not only the pharmaceutical industry but also of research teams all over the world. On the one hand drugs are known for "symptomatic approaches for the treatment of AD" and on the other hand "disease-modifying approaches for the treatment of AD"[30]. Here the focus will be on the second type.

Different stages in the process of amyloid plaque formation have been identified to discover drugs. As described previously APP is cleaved to Aβ. One step in this cleavage is done by β-secretase. There are different types of β-secretase known as BACE-1, normally found in the brain, and BACE-2 commonly found in other organs[31]. As BACE-1 is found mainly in the brain, it seems to be the more important for β-secretase in neurons[32]. As β-secretase does not alter other pathways of APP processing it causes the least intervention on the side of production. But it still has to be taken into account that the function of Aβ is mostly unknown. Therefore changes in production of Aβ might have unwanted side effects.

The same arguments hold for an alternative strategy to reduce the production of Aβ by blocking the γ-secretase. In addition the problem arises that not only the preform of Aβ is a substrate for this enzyme complex, but also other proteins (e.g. Notch receptor)[33]. Therefore not only *blocking* the γ-secretase is considered a suitable way for drug development[3, 34, 35]. As mentioned before the most crucial value for plaque formation is the value of Aβ_{42}/Aβ_{40}. Therefore methods have been developed to alter γ-secretase specifically to produce sorts of Aβ other than Aβ_{42}[36].

As a third possibility a change in α-secretase might alter the pathway. Elevated activity of α-secretase might decrease Aβ production because of competition with β-secretase for the cleavage of APP[37]. Here the major difficulty is to rise the concentration of α-secretase specifically in the compartments where APP is cleaved[38].

As an additional therapeutic strategy immunization via injection of aggregated Aβ plaques[39] was tested successfully as well in in mouse models[40] as in *in vivo* human studies[41, 42].

In this study the focus will be on a strategy not mentioned yet. This is the alteration of Aβ oligomers, the main reason for AD[43]. Once more two different approaches exist. On one hand oligomeric Aβ can be reduced, at the expense of encouraging formation of fibrillar forms[44]. This was shown to improve cognitive function of Aβ overproducing transgenic mice[45]. Or, and this is the main goal of the pre-

sented study, to find inhibitors of the aggregation as already extensively studied by others[10, 18, 46–48]. With both methods shown to have effect[44, 49], it would be better to inhibit aggregation. The problem in speeding up the aggregation is once more the probable loss of function for the Aβ with unknown effects.

1.3. MD simulation

In the field of structural biology different experimental methods have been developed to study biological systems in atomic detail (e.g. Nuclear Magnetic resonance-NMR, X-ray crystallography). But the methods do have their disadvantages; e.g. for X-ray crystals are required and therefore the study of dynamics is difficult. Even with methods like NMR, where time resolution is provided, we find critical motions to be often below its time- and sometimes below its spatial resolution[50]. Therefore computer simulations have been developed. The most frequently used approach is molecular dynamics (MD) simulation. It can be applied to study molecular motions like protein dynamics in detail[51]. On length scales as short as in proteins not only classical mechanics but also quantum mechanics has to be considered. At the beginning this has been done by developing methods to solve the Schrödinger equation. But this is a method limited to only small systems of a few hundred atoms[52]. Instead of solving the Schrödinger equation, MD uses so called force fields (FF) to simulate dynamics of molecules. These FF are used from MD programs and contain the potentials of forces that are applied classically by these programs. One of the most frequently used programs for MD simulations is GROMACS[53–55].
In classical MD simulations the following assumptions are applied in addition to the force field assumption.

Born-Oppenheimer approximation In the Schrödinger equation the motion of nuclei and electrons have to be solved simultaneously. The idea of the Born-Oppenheimer approximation is to separate these parts from each other. This is possible due to the different timescales of motion (e.g. from the point of view of an electron the nuclei are not moving). Electrons move much faster due to their lower mass. This gives separated wave functions which still have to be solved.
In biophysics the interest is upon the motion of the nuclei. Therefore in the force field approach the electron part of the wave function is described by bonded interactions as well as Van der Waals interactions.

For the nuclei an additional simplification needs be made.

Classical description of nuclear dynamics In the force field approach all motions are described via a potential term that gives forces as in the classical mechanics. The parameters for this potentials are given in the force field. Being able to calculate the forces a velocity-verlet algorithm is applied to integrate the equations of motions numerically.

1.3.1. Force fields

Current biomolecular force fields (FF) in use are for example the Amber[56] FF and the Charmm[57] FF. Recent studies show that most of the FFs can reproduce experimental data in a reliable way[58]. The main difference from the technical part between them is the way how to derive the parameters the FFs consist of. But what they have in common is their way to describe the atomistic world. MD simulation programs use the potentials given in the FFs that are classified into (i) bonded interactions (ii) non-bonded interactions and (iii) restraints.

$$\begin{aligned} V(x) &= \sum V_i \\ &= V_{\text{bonded}} + V_{\text{non-bonded}} \end{aligned} \tag{1.1}$$

That means a molecule can either interact with another particle because they are (i) connected via a chemical bond or (ii) they are not connected but exert a long range force like a Coulomb force. Restraints are more artificial and can be applied arbitrarily to any selection of atoms to hold them into a certain relative position.

Bonded interactions

Bonded interactions are interactions of a fixed neighbor list. Bonds are the representation of chemical bonds. All bond interactions are given via a harmonic potential.

$$V_{bonded} = \frac{1}{2}\kappa(x - x_0)^2 \tag{1.2}$$

In this potential x is the current position of one molecule relative to another. This formula shows the need to determine for each pair of molecules an equilibrium state x_0 and a force constant κ. These constants are defined by the FF parameters. In

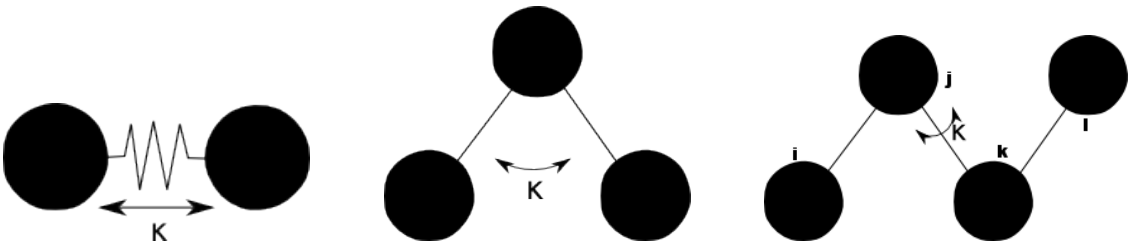

(a) bond (b) angle (c) dihedral

Figure 1.3.: Illustration of the different bonded interactions.

the FF 3 different types of bonded interactions are used. They are named after the restrictions put upon the atoms by them.

Bond potential In the bond interactions 2 atoms are involved. The interaction can be imagined to be due to a spring. Figure 1.3a explains the alternative name bond stretching potential. In this case the parameter x_0 is the distance between the two atoms in equilibrium. κ is a spring constant as known from classical mechanics. It should be mentioned, that even if this potential is the most common there are other potentials for 2-body interactions available. There even exist anharmonic potentials (e.g. Morse potential).
A frequently used approach to bonds is to constrain the bonds, meaning that the bonds can not stretch. This is done using algorithms like LINCS[59] or SHAKE[60].

Angle potential In the angle potential 3 atoms are involved. This interaction is demonstrated in figure 1.3b. Here the given x_0 is the angle between the two bonds formed by the three atoms at equilibrium. The motion induced by this potential is a vibration around the equilibrium state.

Dihedral potential The dihedral potential restricts four atoms into two plains with a certain angle (dihedral angle) to each other. This is demonstrated in figure 1.3c. The two plains are i,j, k and j, k, l. The angle in equilibrium is measured from the so called *cis* state where i and l are on the same side.

Non-bonded interactions

The partners of a non bonded interaction are not given in a fixed list as it is in bonded interactions, but in a list that is updated after a predefined number of

steps. All non bonded potentials are pair additive. The main potentials of the non-bonded interactions are the Lennard-Jones or the Buckingham potential as well as the Coulomb potential.

Lennard-Jones The Lennard-Jones potential is given by

$$V_{LJ} = \frac{c_1}{r^{12}} - \frac{c_2}{r^6} \tag{1.3}$$

Here the parameters c_1 and c_2 have to be determined for every pair of atoms separately. Therefore the FFs have a list of possible combinations where the constants can be looked up. The Lennard-Jones potential describes the interaction of the electron cloud. As the electron cloud can be polarized it has an attractive $1/r^6$ term. On the other hand for short distances the pauli exclusion principle prevents the atoms from getting too close. Is is modelled by the repulsive $1/r^{12}$ term.

Coulomb Coulomb interactions are computationally the most expensive in the simulations. As the range of these interactions is long-range, it can not be neglected at large distances, lead to a computational cost of $\mathcal{O}(N^2)$. This effort is reduced by the so called particle mesh ewald[61] method. It uses the periodicity of the system to calculate the forces in the Fourier space, leading to a computational effort of $\mathcal{O}(N \cdot \log N)$.

Deriving parameters

Even if the way how to derive the FF parameters differs, they have basic strategies in common. Quantum mechanical calculations are carried out to get a first set of parameters. These parameters are further optimized via specific experimental setups. Some force fields are optimized to reproduce specific structural patterns at the expense of others (e.g. some prefer helical structures before beta-sheets). This leads to the problem that not all force fields are equally suitable to study a given problem.

1.3.2. GROMACS algorithms

Without going too much into detail a short introduction to algorithms applied by GROMACS is given here. GROMACS is a simulation software to use the information provided by the FFs to run a MD simulation. The simulated system is prepared

in a suitable box. These boxes have most commonly periodic boundary conditions (pbc). Pbc are used to minimize boundary effects. Therefore the simulated box is considered to be replicated at every boundary. To this box an external pressure and temperature coupling is applied. This is needed because by solving the equations of motion we are naturally in a microcanonical (NVE) ensemble. Physiological conditions are normally at constant temperature and constant pressure. Therefore the coupling algorithms are applied to get into the isothermal-isobaric (NPT) ensemble. For both types of coupling different algorithms are available (e.g. velocity rescaling[62] for temperature and Parrinello-Rahman[63] for pressure). In addition GROMACS provides a variety of tools to analyze the files created during the MD simulation.

1.3.3. Limitations

Due to the applied assumptions, limitations are encountered in this approach that are not present in the quantum mechanical calculations. For example, if a bond is described via a harmonic potential it can never break. Nor is there a possibility to form new bonds. Therefore chemical reactions can not be described via the FF approach.
Furthermore due to numerical integration errors might occur if the integration timestep is chosen too large.

For a further introduction on MD implementation and methodology see[64].

1.4. Ligands

From *in vitro* studies performed by C. Griesinger et al. (NMR-based Structural Biology, Max-Planck-Institute for Biophysical Chemistry) two small molecules (for structure see figure 1.4) that can inhibit full length Aβ aggregation are known.
For the first ligand two different protonation states of the nitrogens are known, populated 1:1. One of the nitrogens is always protonated while the other is not. This is a drawback as in MD studies the protonation state must be defined at the beginning of the simulations. Therefore to simulate the system as close as possible to an *in vitro* experiment, the ligands are always simulated as pairs with one of them being in one protonation state while the other is in the other protonation state.

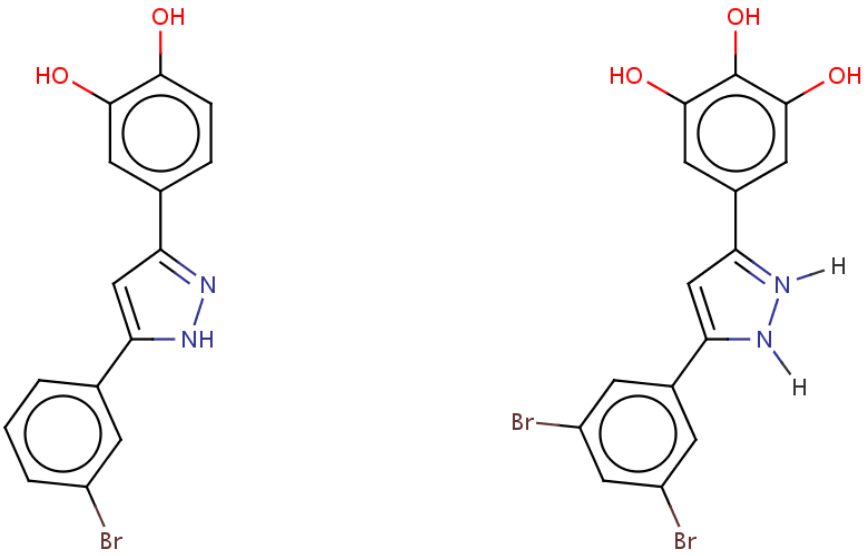

(a) Ligand 1 (b) Ligand 2

Figure 1.4.: The ligands simulated in the system.

For the second ligand the protonation state is unambiguous. This is one of the reason to put the focus on the second ligand.
Another important difference to the first ligand is the charge. While the first ligand is uncharged, the second ligand carries a positive net charge.

2. Methods

2.1. System overview

An overview of the simulated systems is given in table 2.1. The steric zipper peptides with sequences ^{16}KLVFFAE^{22} and ^{30}AIIGLM^{35} were simulated with (3 simulations each) and without ligands (1 simulation for each peptide ligand combination, explanations to the ligands are given in section 1.4), in the Amber FF as well as in the Charmm FF. In addition the simulations without the ligands are also carried out with preformed beta-sandwich structures (instead of ^{16}KLVFFAE^{22}, ^{16}KLVFFA^{21} was used).
The ^{16}KLVFFA^{21} (instead of ^{16}KLVFFAE^{22}) peptide was also simulated with a single ligand of type 2 (5 simulations) using the Charmm FF. Furthermore one of the preformed structures of ^{16}KLVFFAE^{22} is chosen (with intermediate stability) after 100 ns. This structure is the basis for a new simulation with 12 additional ligands of type 2.

2.2. Starting structures and topologies

In order to impose no bias to the aggregation the following protocol was applied to set up the simulations. Alternatively, the starting structures of monomeric peptides were created using PYMOL[65]. To these structures CONCOORD[66] was applied to generate an ensemble of 1000 randomly twisted peptides. CONCOORD only considered topological constraints.
The preformed structures were constructed based on crystal structures from the PDB. For Aβ_{16-21} the three different forms 2Y2A, 3OW9, 2Y29 and for Aβ_{30-35} 2Y3J were considered[15].

The topologies for the ligands in the Amber FF have been created using antechamber[67] (Creation of structure and topology was carried out by Vytautas Gapsys (Depart-

Force Field	Peptide (#, conc.)	Ligand (#, conc.)	Information
Amber & Charmm	Aβ_{16-22} (12, ~20 mM)	×	3 simulations
Amber & Charmm	Aβ_{30-35} (12, ~20 mM)	×	3 simulations
Amber & Charmm	Aβ_{16-21} (12, ~20 mM)	×	preformed, 3 different formes
Amber & Charmm	Aβ_{30-35} (12, ~20 mM)	×	preformed
Amber & Charmm	Aβ_{16-21} (12, ~20 mM)	Ligand 1 & 2 (12, ~20 mM)	†
Amber & Charmm	Aβ_{30-35} (12, ~20 mM)	Ligand 1 & 2 (12, ~20 mM)	†
Charmm	Aβ_{16-22} (12, ~20 mM)	Ligand 2 (1, ~1.7 mM)	5 simulations
Charmm	Aβ_{16-21} (12, ~20 mM)	Ligand 2 (12, ~20 mM)	continued preformed after 100 ns

Table 2.1.: Overview of the simulated systems. ×: simulation systems without ligands, †: no additional information

ment of Theoretical and Computational Biophysics, Max-Planck-Institute for Biophysical Chemistry)). In addition sigma holes[68, 69] were applied to the bromine atoms.

Ligand topologies compatible with the Charmm FF were created using the SwissParam fast force field generation tool[70]. An ensemble of 100 ligand structures in a random conformation was generated using tCONCOORD[71], considering only topological constraints.

For all systems, monomeric peptides and ligands are chosen randomly from the previously calculated ensembles and placed randomly in a cubic box of 1000 nm^3. In addition explicit solvent and ions in a concentration of 0.15 M were added. The protonation states for all systems were at pH 7.

2.3. MD Setup

All MD simulations were carried out using GROMACS version 4.5.5[53–55]. The force fields used were the Amber ff99SB*-ILDN[56] and the Charmm36[72] together with the TIP3P water model[73]. All bonds were constraint using LINCS[59]. The velocity-rescaling[62] algorithm was applied to couple the simulation system to an

external heat bath with a temperature of 300 K using a time constant of $\tau = 0.1$ ps. For pressure coupling the scheme of Parrinello-Rahman[63] was used to hold the system at a pressure of 1 bar. Initial velocities were taken according to a Maxwell-Boltzmann distribution at 300 K. All simulations were carried out with periodic boundary conditions applied to the simulation box. Prior to the simulations, energy minimization was applied.

2.3.1. Amber FF

Virtual sites[53] were used to increase the time-step to 4 fs while maintaining energy conservation. The neighbor list was updated every 3 steps. The neighbor list cut-off was chosen as $r_c = 1.0$ nm. For further electrostatic forces Particle Mash Ewald (PME) was applied with a cut-off of $r_c = 1.0$ nm[61]. The VdW-type was chosen to be Switch with a cut-off of $r_c = 1.0$ nm and a total cut-off of 1.2 nm. In the Amber FF a time constant of $\tau = 1$ ps was applied.

2.3.2. Charmm FF

The time-step was set to 2 fs. The neighbor list was updated every 10 steps. The neighbor list cut-off was set at $r_c = 1.4$ nm. Here also PME was applied with a cut-off of $r_c = 1.4$ nm[61]. For VdW-type a cut-off was used with a cut-off range of $r_c = 1.0$ nm. For the Charmm FF a time constant of $\tau = 4$ ps was used.

3. Results and discussion

3.1. Association

It is known that the Aβ segment ^{16}KLVFFAE^{22} is an aggregating sequence[15]. This segment is simulated in the Charmm FF as described in chapter 2. For all three simulations carried out (in the figures referred to as trails) aggregation is found for this peptide. In figure 3.2 the clustering behavior is plotted as a function of time. Here peptides closer together than 0.4 nm are considered to form a cluster. If an additional peptide is within a distance of 0.4 nm of a peptide in a cluster, this additional peptide is considered a member of the same cluster. The cluster assignment is color coded in the figure. At the beginning the monomers almost immediately start to aggregate. The aggregation pathway is through a variety of oligomeric intermediates.
After 100 ns the majority of the peptides are part of an aggregate. Some individual peptides can still be found in a monomeric state or in independent clusters, but the majority can be found within one cluster. In the later progress, patterns of smaller aggregates can be found for short times (e.g. at the end of trail 1).

The fast growth in a variety of smaller oligomers (later forming one single cluster) is contrary to the mechanism suggested by the seeding hypothesis, in which the major barrier for aggregation is suggested to be the formation of a seed [74, 75]. One reason might be that for the full length Aβ it is necessary to have a sequence accessible that can form oligomers. These sequences need to be accessible simultaneously for all interacting peptides at the time of their encounter. Because of the fewer number of residues in this studied fragment this is always given in an encounter of the examined peptide.
The pattern of smaller aggregates in the later part of the simulations arises due to internal reformation. By visual inspection of the trajectories a disassembly was not observed. The clustering algorithm used for figure 3.2 however shows oscilla-

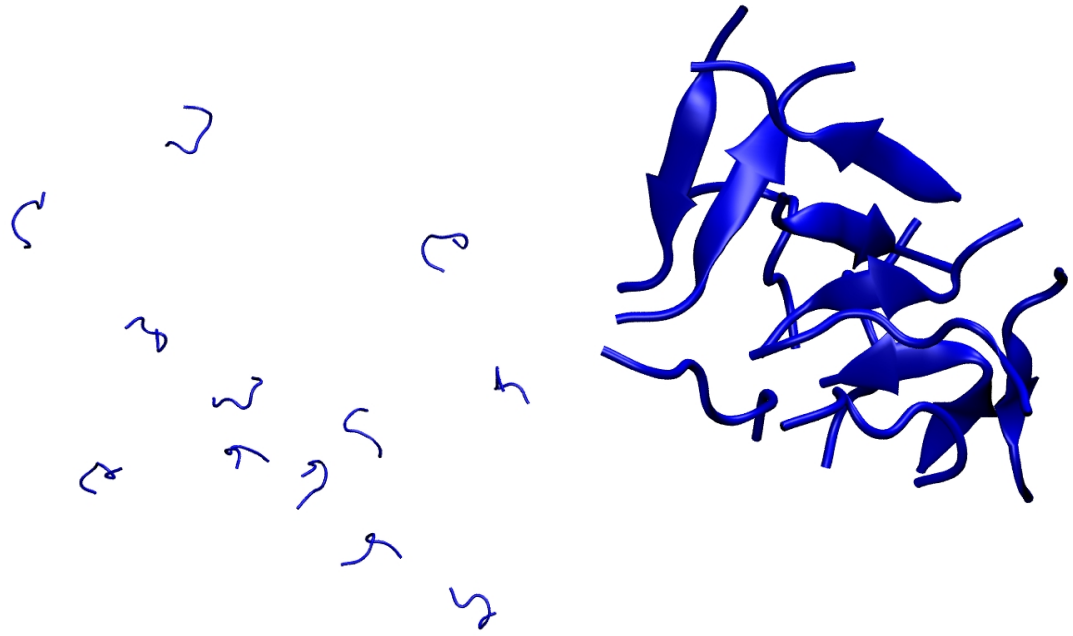

(a) At the beginning (b) After 500 ns

Figure 3.1.: The ^{16}KLVFFAE^{22} peptide simulated in the Charmm FF. At the beginning 12 peptides are distributed randomly in a box. During the simulation they form a cluster and arrange into beta-sheets.

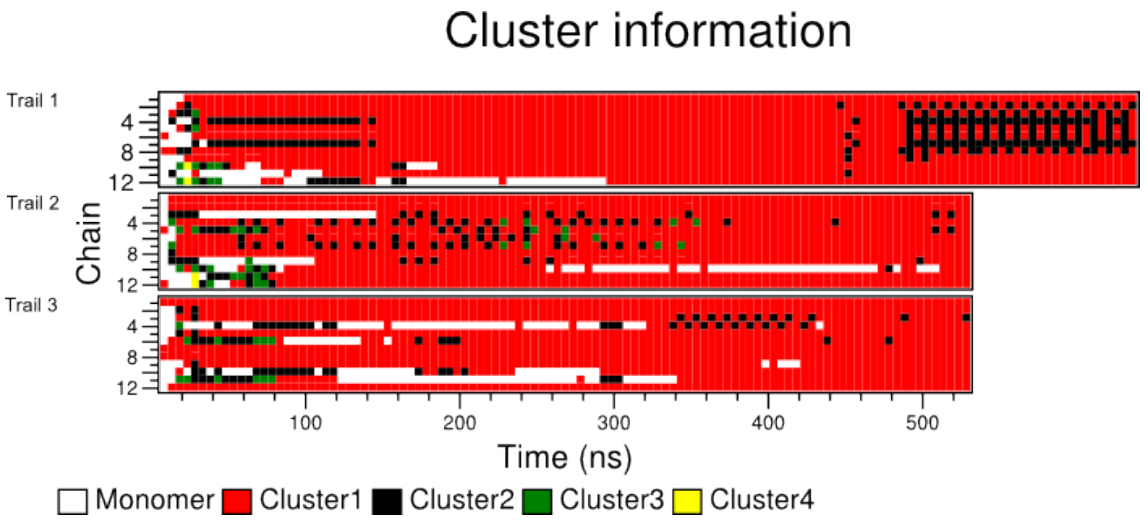

Figure 3.2.: Clustering behavior over time of ^{16}KLVFFAE^{22} in the Charmm FF. The same color represents the belonging to the same cluster. A peptide is defined to be in a cluster if the distance to a peptide in the cluster is less than 0.4 nm.

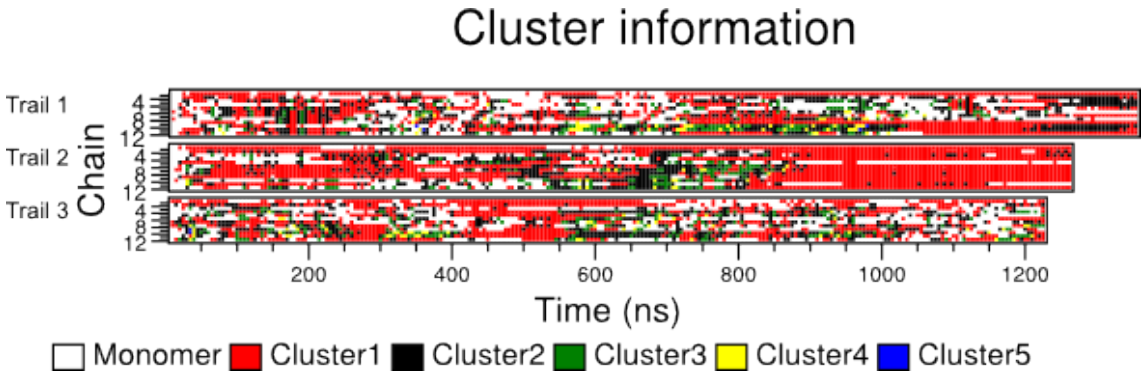

Figure 3.4.: The clustering behavior of the ^{16}KLVFFAE^{22} peptide in the Amber FF. For further explanation see figure 3.2.

tory behavior, suggesting transient disassembly. This may be due to the applied cut-off distance in the cluster definition. For further simulations a new definition of clusters with another distance should be considered to create the cluster figures, matching the behavior seen by visual inspection.

The same simulations are carried out with the Amber FF to find out how differences in the force fields affect the aggregation behavior. This is important to separate effects that are exclusively found due to force field parameters.

In the Amber FF the aggregation is frequently limited to few peptides (see figure 3.4). These aggregates are mostly unstable. Only in one of the simulated systems a larger aggregate forms that appears to be stable (at the end of trail 2 in figure 3.4). In other simulations (e.g. trail 3 after 450 ns) larger aggregates form as well. But in the contrast to the simulations in the Charmm FF they disassemble rather fast.

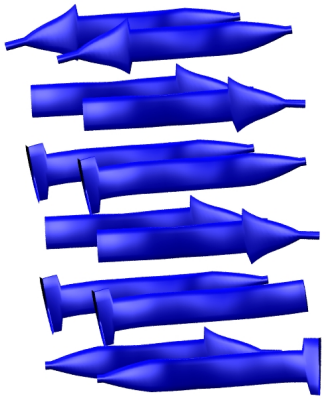

Figure 3.3.: A beta-sheet structure of a ^{16}KLVFFA^{21} crystal from NMR data. (PDB: 2Y2A)

Comparing the aggregation in the Amber FF to the previously described behavior in the Charmm FF, a difference in speed and frequency of aggregation is observed. (compare figures 3.2 and 3.4). While clusters in the Charmm FF, once formed, rarely start disassembling and mostly reform, this

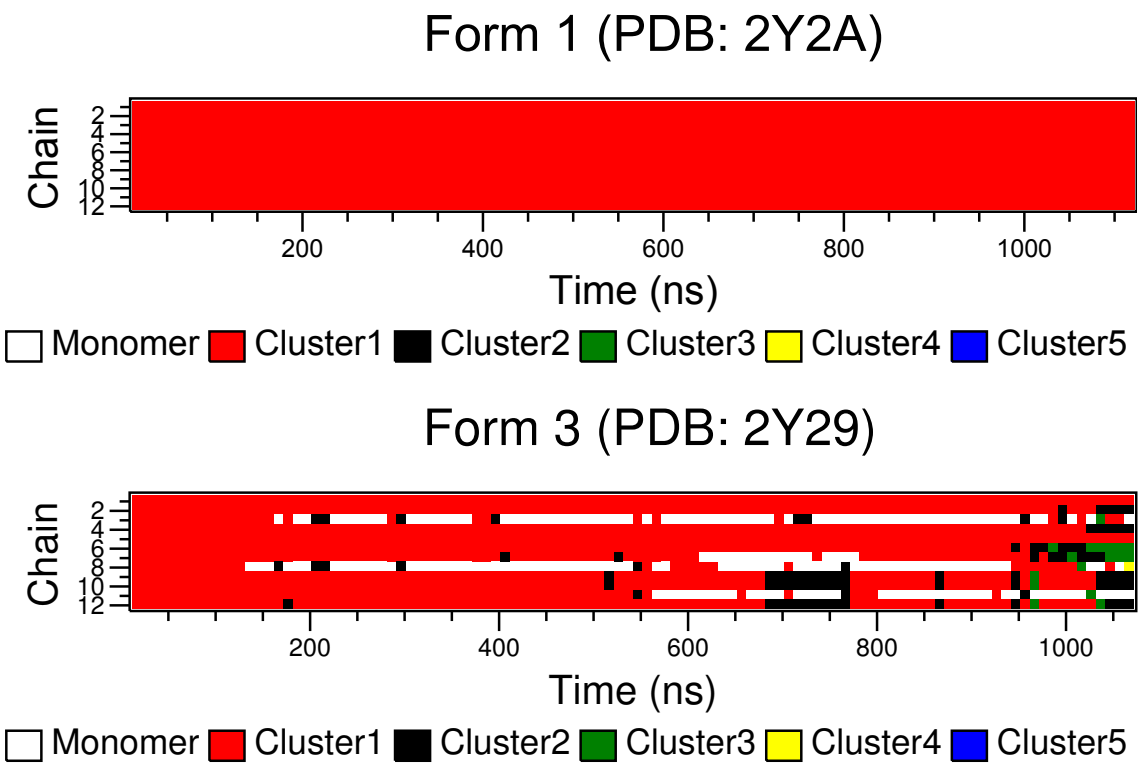

Figure 3.5.: The clustering behavior of preformed structures of the ^{16}KLVFFA^{21} Aβ segment simulated in the Amber FF. The starting structure is a dry steric zipper consisting of 12 peptides. The structure is a fragment from a crystal structure. For further explanation see figure 3.2.

behavior is not observed for the simulations performed with the Amber FF, where clusters frequently form and disassemble.
Thus, for this sequence, the Charmm FF shows a greater aggregation-propensity than the Amber FF.

In addition, simulations have been carried out with preformed structures taken from crystal fragments[15]. These structures are simulated in the same setup as used for the randomly distributed peptides. The observed behavior of these simulations is distinct among the different initial structures. While the simulations carried out in the Charmm FF do not show disassembly for any of the starting structures, in the Amber FF one of the structures disassembles to the major part while one stays aggregated(see figure 3.5).
This might suggest that in the Amber FF the initial arrangement of the aggregate is important. For the assembly simulations the behavior of the preformed structures

implies that the stable aggregate first has to be reached from the random starting structure. The variety of aggregates described by Colletier et al.[15], of which some seem to be unstable, may explain the aggregation behavior observed in the Amber FF: If unstable aggregates form in the simulation with the randomly distributed starting structure they will disassemble again.

To quantify this behavior it would be of interest to compare the spontaneously formed structure that was found to be stable in the Amber FF with the stable pre-formed aggregate using a Root Mean Square Deviation (RMSD) analysis. The provided hypothesis would be supported if the RMSD of the aggregated structure formed in the simulations with a random starting configuration would be smaller for the preformed structure found to be stable, than to structures found to be unstable.

The disassembly of preformed structures was not observed in the Charmm FF. For all three simulated preformed structures (2Y2A, 3OW9 and 2Y29) exclusively relaxation but no disassembly was observed.

These findings lead to the choice of the Charmm FF as the FF for the majority of the simulations to be carried out to study aggregation, and the putative effect of inhibition.

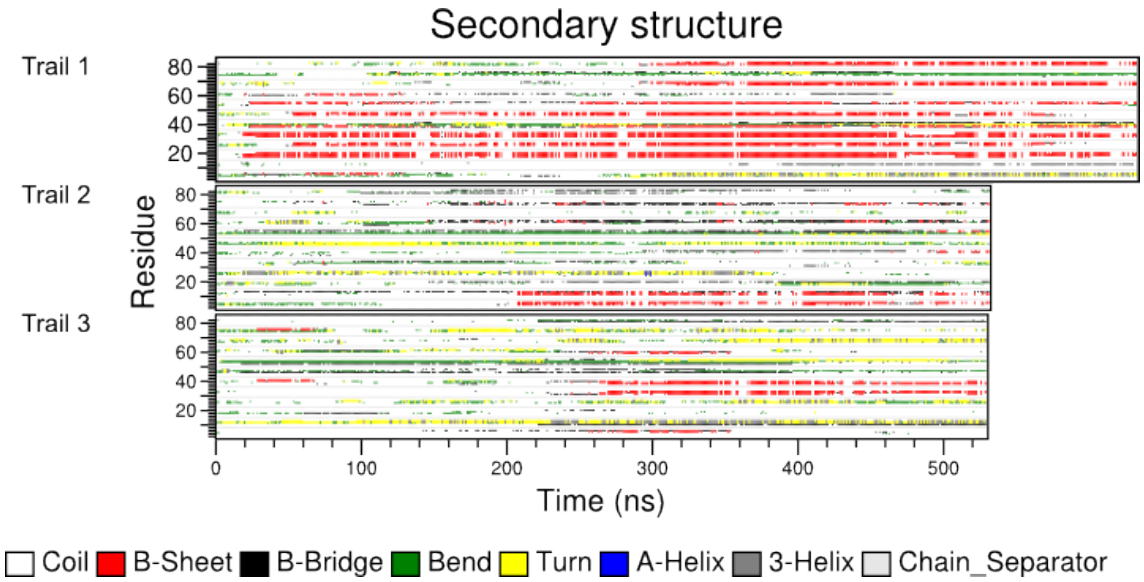

Figure 3.6.: Secondary structure as a function of simulation time for ^{16}KLVFFAE^{22} in the Charmm FF calculated by DSSP[76]. The vertical coordinate represents the residue number (1 is the first residue of one of the peptides, 8 is the first residue of the next peptide, and so on). The secondary structure is color coded.

3.2. Secondary structure

As a second observable the secondary structure is of interest. It is known that the amyloid fibrils grow due to the formation of a backbone consisting of beta-sheets[16]. The used fragment is known to form such a beta-sheet *in vitro*[15].

For the simulations in the Charmm FF the secondary structure is inhomogeneous throughout the different simulations (see figure 3.6). While the first simulation shows a high beta-sheet content, the other simulations do not. In the second and third simulation other secondary structure elements, like bend and turn, are appearing more frequently. This large inherent spread indicates that it will be challenging to derive statistically significant differences due to e.g. FF or inhibition effects. Contrary to the aggregation behavior, the formation of beta-sheets can also be found in a later point of simulation.

What is of special interest is the difference between the simulations. Comparing the secondary structure to the aggregation behavior a correlation between beta-sheet content and stability is apparent. As beta-sheets are very rigid structures due to intra-chain hydrogen bonds it is evident that the rearrangement of them is limited. Therefore it gets apparent why the first simulation shows a higher packing (see figure

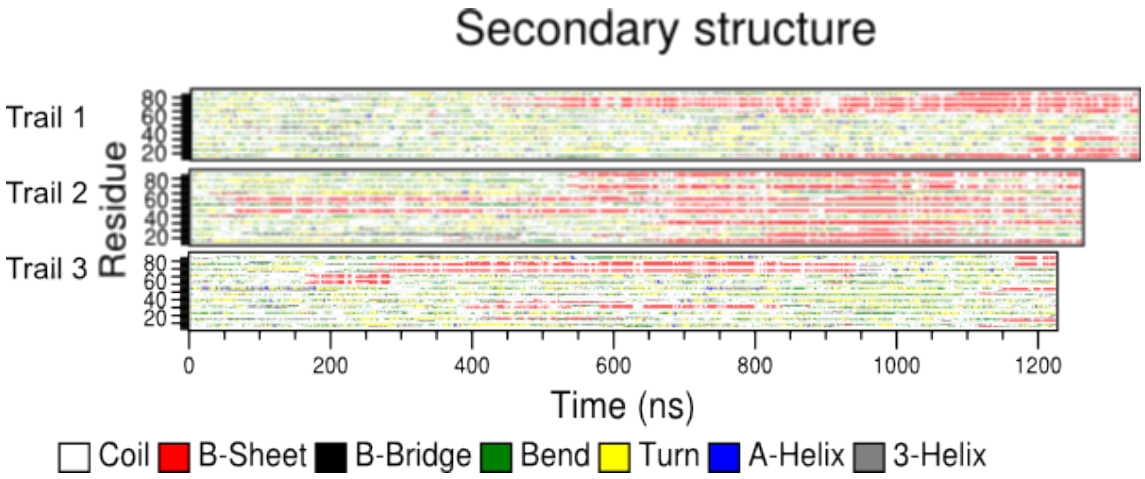

Figure 3.7.: The secondary structure elements over time for the^{16}KLVFFAE^{22} peptide in the Amber FF. For further explanation see figure 3.6.

3.2) than the others do. From the rearrangements it is suggested that the simulations have not reached the absolute minimum of the free energy landscape yet. This should be the fully aggregated state[77], most probably a dry steric zipper as found in *in vitro* studies[15].

The additional simulations carried out in the Amber FF also show a variety in secondary structure elements. Beta-sheet formation was obsered in all simulations. In the second simulation the beta-sheet content is much higher than in the other simulations in which other secondary structure elements, like bend and turn, are more common.
Compared to the Charmm FF none of the observed differences are statistically significant. However it is apparent that in the Amber FF the secondary structure forms more slowly than in the Charmm FF. But this can also be exclusively due to statistics and is not necessarily due to systematical reasons. This is quite surprising, seeing that the aggregation behavior differs significantly in the two FF.
Comparing the aggregation behavior more closely to the secondary structure, it seems that aggregates once formed in the Amber FF, do adopt a beta-sheet secondary structure much faster than they do in the Charmm FF.

3.3. Changes due to ligand interaction

To see the effect of the ligands on the aggregation, the ligands are simulated in a ratio of 1:1 with the peptides (for further explanations see section 2). Focusing on the aggregation (see figure 3.9a) the simulations carried out with the first ligand show two separated clusters which unify in the later simulation. In the case of the second ligand the simulation shows a pathway of growth through encounters of dimers and a rapid growth to the full length structure (an example structure from the simulations is shown in figure 3.8). For both systems all peptides and ligands form a single aggregate after 100 ns.
The aggregation goes through the aggregation of ligands with peptides as well as ligand-ligand and peptide-peptide aggregation. Neither of them seems to be preferred.
Comparing this to the aggregation of ^{16}KLVFFAE^{22} without ligands (see figure 3.2) these seems to be not significantly different. In addition the differences between the simulations with the two ligands might be due to limited statistics and not systematic. To validate this further, additional statistics (simulating the same system more frequently) would be necessary.

Looking at the secondary structure a very different effect of the two ligands was found. For the first ligand the secondary structure consists mostly of beta-sheets. These form during the simulation with the ligands in the same cluster. Residues that are not within a beta-sheet are mostly adopt coil conformation. For the second ligand a variety of secondary structure elements like turns and bend is observed, but beta-sheets are almost not forming. Only between 220 and 300 ns, a beta-sheet was observed.
The change of secondary structure seems to be significant enough to suggest an effect due to the ligands. Especially looking at the difference between the secondary structure seen for the two ligands, an effect is probable. The first ligand seems to prohibit formation of secondary structure elements like turns and coil while encouraging the growth of beta-sheets and for the other parts remaining in coil. The exact opposite effect seems to be introduced by the second ligand. Here the arrangement into turns and bend seems to be encouraged while the growth of beta-sheets is prevented.

Interaction energies might elucidate the difference between the simulations with the

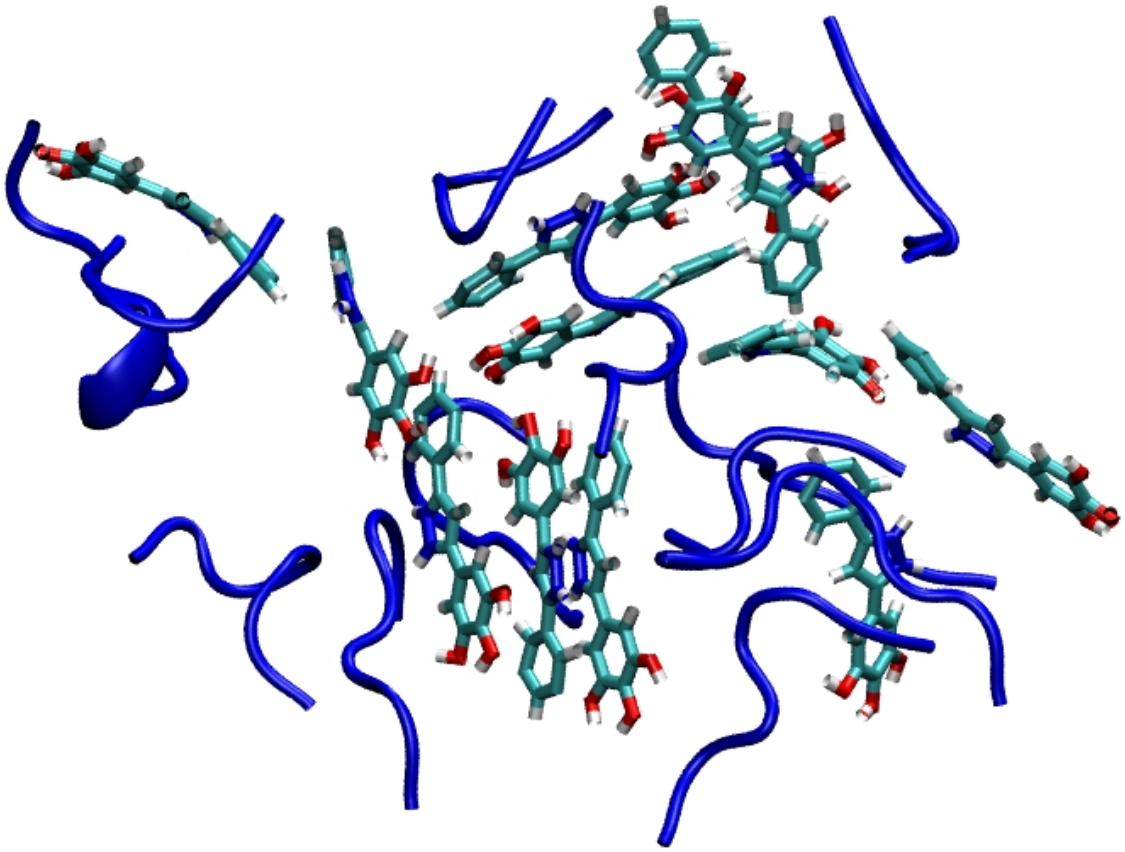

Figure 3.8.: Aggregate of Aβ segment ^{16}KLVFFAE^{22} and ligand 2. Shown is a configuration reached after 420 ns of simulation. The setup were randomly chosen starting positions for ligands and peptides.

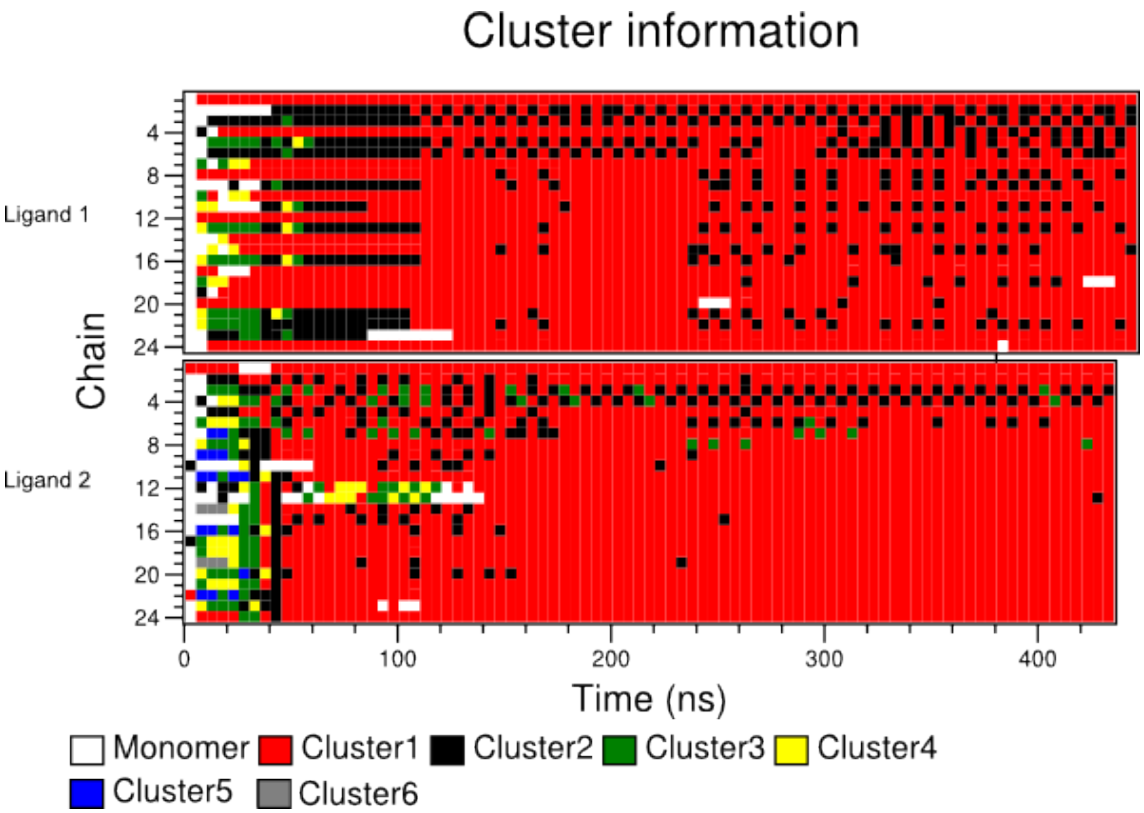

(a) Clustering behavior. Number 13 to 24 are the ligands.

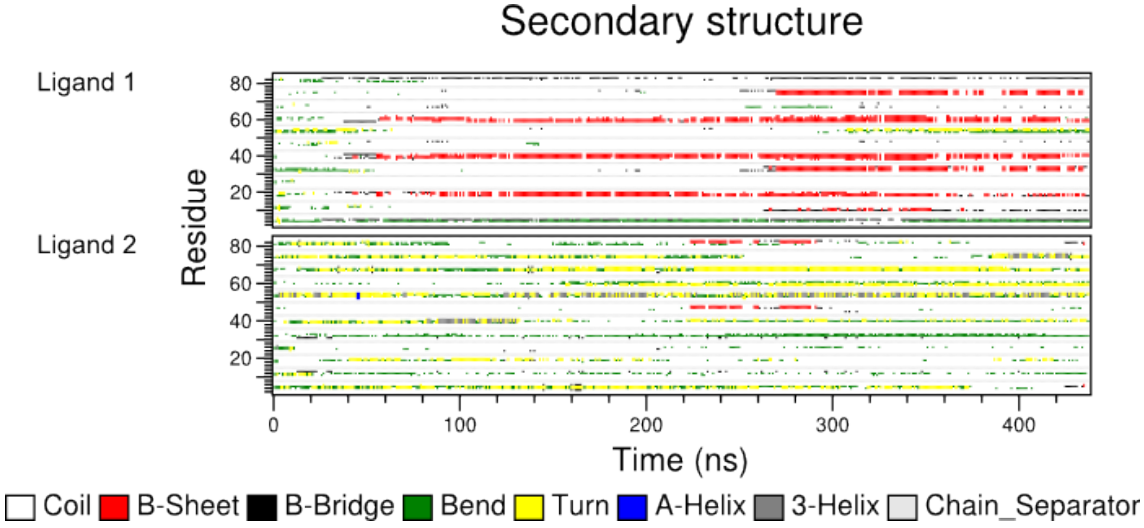

(b) Secondary structure

Figure 3.9.: The ^{16}KLVFFAE^{22} peptide simulated in the Charmm FF, with additional ligands. The ratio of ligands to peptides is 1:1. Compare to figures 3.2 and 3.1a For further information see figures a) 3.2 and b) 3.6.

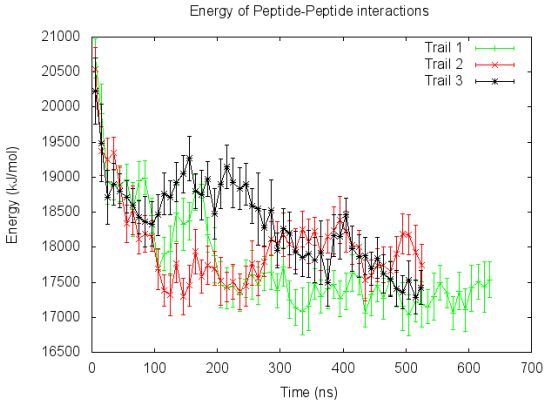

(a) peptide-peptide interaction energy without ligands

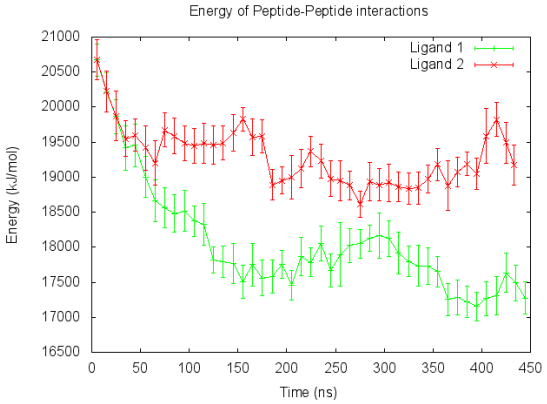

(b) peptide-peptide interaction energy with ligands

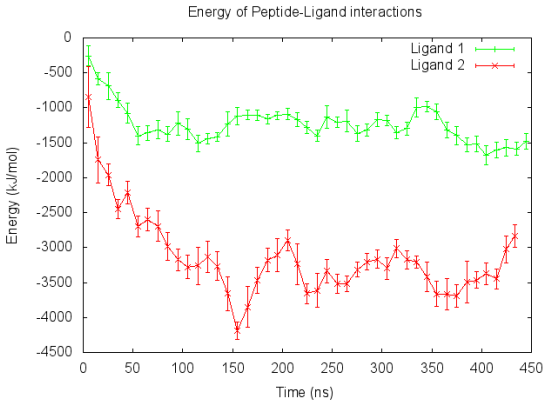

(c) ligand-peptide interaction

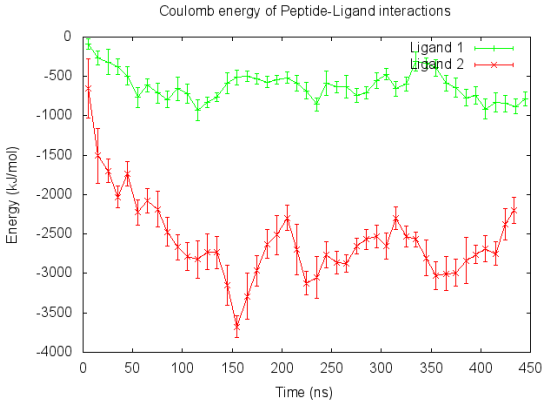

(d) coulomb energy for ligand-peptide interaction

Figure 3.10.: The ^{16}KLVFFAE^{22} peptide simulated in the Charmm FF. Shown is the change of energy over time. The energies have been calculated using the g_energy tool from the GROMACS software package[53–55]

different ligands as well as between the simulations with the ligands and without. Without ligands a significant drop of energy of the peptide-peptide interaction is observed for all simulations (see figure 3.10a). In all of the simulations the energy drops around 2500 kJ/mol during the first 450 ns.
For simulations with ligands the energy starts at the same value as in the case without ligands. The simulation of the first ligand does not show a significant difference in the peptide-peptide energy from the simulated systems without ligands (see figure 3.10b). For the second ligand the energy of the peptide-peptide interaction changes less from the beginning of the simulation to its end. This difference between the simulations without ligands and with ligands is around 2000 kJ/mol.
Additionally, ligand-peptide interactions have been analyzed for the simulations with ligands (see figure 3.10c). Here a large change in energy between the starting configuration and the end configuration is visible for the second ligand. The first ligand, almost starting at the same energy, does not show a change as significant as the second ligand. Here, the differences of the peptide-ligand interaction energy is around 2000 kJ/mol. Interestingly, the same pattern was observed looking only at coulomb interactions of the peptides with the ligands (see figure 3.10d). This change in energy shows again differences between the first ligand and the second one. It therefore seems as if the change in the peptide-peptide energy observed for ligand 2 is due to the compensating energy of ligand-peptide interactions.
Large differences between the ligands were found although the ligands are quite similar. The main difference between them is the charge carried by the second ligand. This leads to the major difference as indicated by the coulomb interaction energy. ^{16}KLVFFAE^{22} carries two charged residues. These are the positively charged lysine(K) and the negatively charged glutamic acid(E). In addition the N- and C-termini carry charges.
To determine the effect of the charged residues, a suggested analysis would be the determination of the residues mainly interacting with the peptide.

As simulations with another peptide have already been carried out, this might also be a possibility to find out the effect of charged interactions. This is done for the ^{30}AIIGLM^{35} Aβ segment, with neutral side chains.
The secondary structure of the simulations without the ligands is inhomogeneous. The first simulation adopts a large number of beta-sheets, while the other simula-

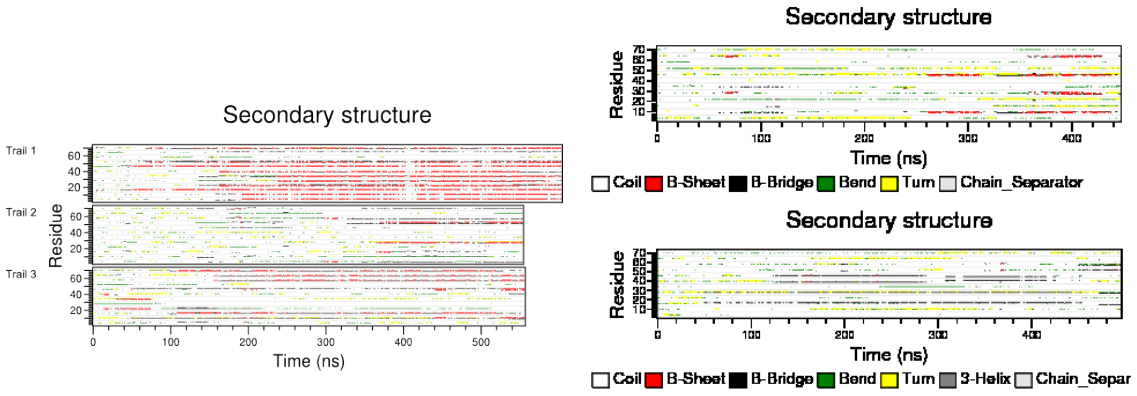

(a) simulations without ligands (b) simulations with ligands

Figure 3.11.: Secondary structure of ^{30}AIIGLM^{35} in the Charmm FF. For the simulations with ligands the upper graph shows the behavior with the first ligand, the lower one shows ligand 2. For further information see figure 3.6

tions adopt rather other conformations (see figure 3.11a).

While the simulation with the first ligand shows a low propensity to form beta-sheets, the simulations with the second ligand do not show beta-sheets but only beta-bridges.

Although this pattern would be consistent with the change of peptide-peptide interaction as previously mentioned, the change due to the ligand is not significant. Both of the secondary structures found in the simulations with the ligands are within the range of diversity found for simulations without ligands.

The peptide-peptide interaction energy drops for this segment as aggregation progresses in the case without any ligands (see figure 3.12a). This is comparable to the ^{16}KLVFFAE^{22} peptide. But for ^{30}AIIGLM^{35} the interaction seems to be more inhomogeneous than for ^{16}KLVFFAE^{22}.

The peptide-peptide interaction energies for the simulations with ligands (see figure 3.12b) decrease during the simulation. While this was also found for the other peptide, the difference is that both energies drop almost equally. No significant difference between the two ligands is observed in the energies.

The ligand-peptide interaction energy (see figure 3.12c) decreases over time for both ligands. For both ligands it seems to reach almost an equilibrium state with ligand 2 showing a strong interaction. An energy difference of around 1500 to 2000 kJ/mol between the ligands is observed at the end of the simulation. This difference is similar to the difference found for the other peptide: A similar drop in coulomb energy

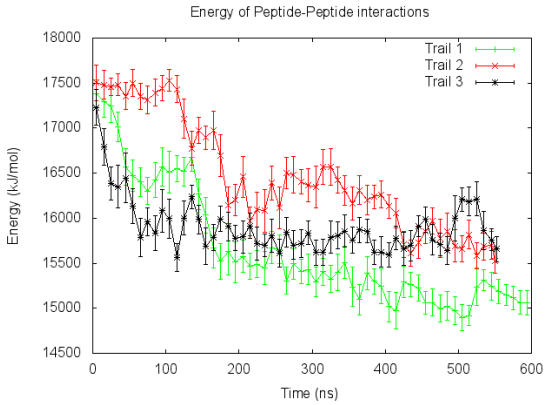

(a) Energy of peptide-peptide interactions without ligands.

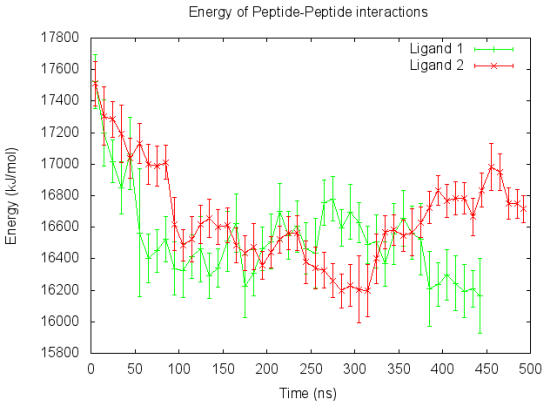

(b) Energy of peptide-peptide interactions with ligands.

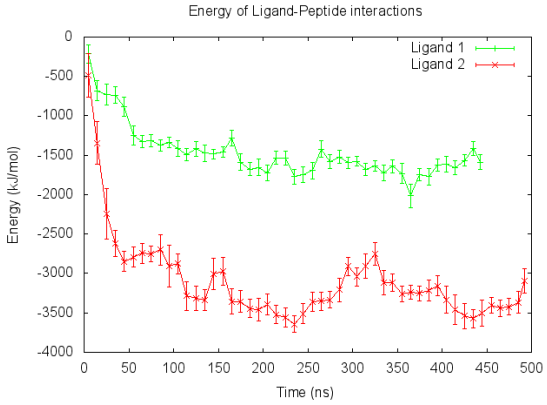

(c) Energy of ligand-peptide interaction.

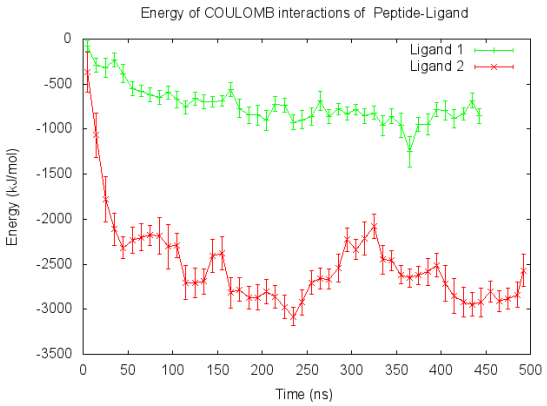

(d) Coulomb energy of ligand peptide interaction.

Figure 3.12.: Energy of ^{30}AIIGLM^{35} in the Charmm FF. For further information see figure 3.10.

as in the case of the ^{16}KLVFFAE^{22} peptide is observed (see figure 3.12c).
The observed interactions lead to the suggestion that the majority of interaction is due to coulomb energy. The similarity in the behavior of the peptides with and without charged side chains suggests that the charged second ligand does not interact with the charged side chains but rather with the charged termini.

It seems as if the interaction with termini, that is suggested as charged interaction for the second ligand with the ^{30}AIIGLM^{35} segment, does not change the energy of peptide-peptide interaction. This suggests that in the process of beta-sheet formation the charged termini do not play a major role. The coulomb interactions of the first ligand with the ^{16}KLVFFAE^{22} peptide has a change of energy comparable to the ligand free case, while the peptide-peptide interaction seems to be reduced. This leads to the suggestion that the interaction of the ligand with this peptide might be predominantly with the charged side chains.

As the beta-sheet structure is formed by hydrogen bonds it is of interest to analyze on the hydrogen bond energies (see figure 3.13). In the simulations with the ^{16}KLVFFAE^{22} peptide a drop of hydrogen bond energy between the peptides is observed upon aggregation. The drop of hydrogen bond energy for peptide-peptide hydrogen bonds is also observed in simulations with this peptide and the first ligand. For simulations with the second ligand and this peptide the hydrogen bond energy between the peptides is less pronounced. The peptide-ligand hydrogen bond energies in the simulations with ^{16}KLVFFAE^{22} and the ligands shows the opposite trend. For the first ligand the interaction is weaker than for the second ligand.
The change in the hydrogen bond energies suggests competitive inhibition by the second ligand for hydrogen bonds between the ^{16}KLVFFAE^{22} peptides.

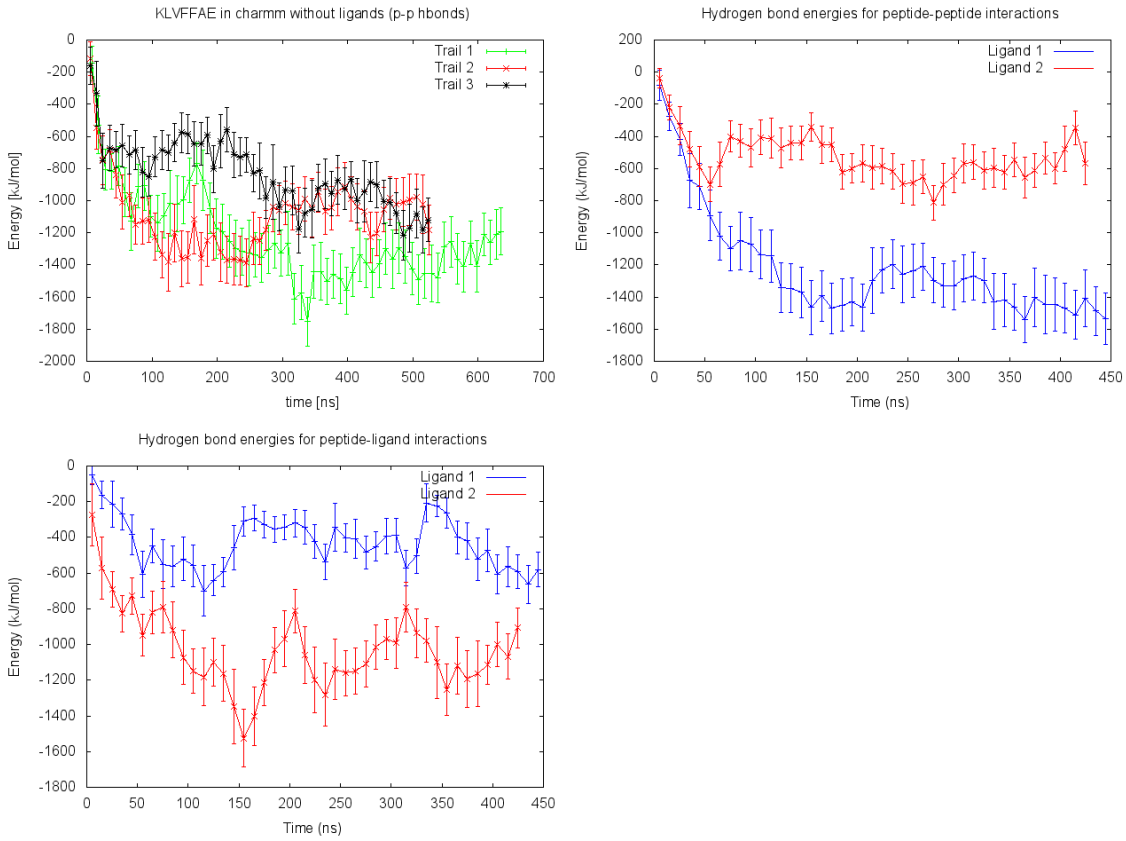

Figure 3.13.: Hydrogen bond energies for the ^{16}KLVFFAE^{22} peptide with and without ligands simulated in the Charmm FF.

4. Conclusions and outlook

4.1. Conclusions

In the presented study simulations with the Aβ fragments ^{16}KLVFFAE^{22} and ^{30}AIIGLM^{35} were carried out. Furthermore, simulations with a combination of 12 peptides of one type and small molecules known to inhibit full length Aβ aggregation were performed. To reduce the bias introduced through force field parameters the two FF Amber and Charmm were applied to some of the simulations.

From the simulations of ^{16}KLVFFAE^{22} in the Charmm FF no prevention of aggregation was observed due to the addition of ligands. Instead, a change of secondary structure through the ligand interaction was observed. While the mechanism of interaction stays mostly unrevealed for the first ligand, the charge of the second ligand probably is the key player in the interaction between this ligand and the ^{16}KLVFFAE^{22} peptide.
Comparing the secondary structure and energies of the interaction of the ^{16}KLVFFAE^{22} peptide with the second ligand to those for the interaction between ^{30}AIIGLM^{35} and the second ligand, the charged residues of the ^{16}KLVFFAE^{22} Aβ fragment seem to be of importance for the peptide-peptide interactions.
The change of hydrogen bond energies between the ^{16}KLVFFAE^{22} peptides suggest a competition for hydrogen bonds as a mechanism contributing to inhibition. This is a possible explanation for the observed change in secondary structure.

One might speculate that the growth of ^{16}KLVFFAE^{22} into a steric zippers is inhibited at least by the second ligand. Here peptide-ligand interactions disrupt the secondary structure. This does not have an effect on the aggregation of oligomers as small as dodecamers but might prevent formation of fibrils.

4.2. Outlook

To verify the change in interactions (i.e. coulomb and hydrogen bonds) between the second ligand and the ^{16}KLVFFAE^{22} peptide more statistics is needed. Therefore, additional simulations should be carried out with the ^{16}KLVFFAE^{22} peptide together with (i) the second ligand and maybe also with (ii) the first ligand, in the same setup as before.
It might be that careful evaluation of the already available simulations with ^{16}KLVFFAE^{22} and the second ligand in a ratio of 12:1 reveal additional information on the analyzed observables (e.g. hydrogen bonds, interaction energy) to confirm systematic changes of hydrogen bond and coulomb energies.
To reveal if peptide-ligand interactions (i.e. coulomb and hydrogen bonds) are strong enough to disassemble preformed structures, the simulations with preformed structures of ^{16}KLVFFA^{21} and the added second ligand (not described extensively here) should be prolonged. As a control the simulation without the ligands also would need to be prolonged to the same time.
As coulomb interactions seem to be key in the peptide-ligand interactions of ^{16}KLVFFAE^{22} and the second ligand, electrostatic properties of the system could be changed to test this hypothesis. Therefore, a possible idea is to apply an additional charge to the second ligand, thereby giving it a neutral net charge. Another possibility would be to change the ion concentration of the system. Increased ion concentration should lead to a decrease of long range coulomb interaction due to shielding effects.

A. Acknowledgments

I would like to thank Bert de Groot for giving me the opportunity to be part of the department and introducing me to the field of computational biophysics. His guidance is the reason for the success of this thesis.
I would also like to thank Dirk Matthes for having advises even being mostly far away.
Special thanks to Martin Vesper and Hadas Leonov for not getting tired to answer my questions.
In addition I would like to thank Vytautas Gapsys for his help. And all others of the group for giving me a hand if needed.

Bibliography

[1] Christopher M. Dobson. Protein folding and misfolding. *Nature*, 426(6968):884–890, December 2003. A general introduction to protein folding and misfolding. Writen as a review. Short part of amyloid formation.

[2] Christian Haass and Dennis J. Selkoe. Soluble protein oligomers in neurodegeneration: lessons from the alzheimer's amyloid [beta]-peptide. *Nat Rev Mol Cell Biol*, 8(2):101–112, February 2007.

[3] Dennis J. Selkoe. Alzheimer's disease: Genes, proteins, and therapy. *Physiological Reviews*, 81(2):741–766, 2001.

[4] M Shoji, TE Golde, J Ghiso, TT Cheung, S Estus, LM Shaffer, XD Cai, DM McKay, R Tintner, B Frangione, and al. et. Production of the alzheimer amyloid beta protein by normal proteolytic processing. *Science*, 258(5079):126–129, 1992.

[5] M. S. Cheon, M. Dierssen, S. H. Kim, and G. Lubec. Protein expression of bace1, bace2 and app in down syndrome brains. *Amino Acids*, 35:339–343, 2008.

[6] PH St George-Hyslop, RE Tanzi, RJ Polinsky, JL Haines, L Nee, PC Watkins, RH Myers, RG Feldman, D Pollen, D Drachman, and et al. The genetic defect causing familial alzheimer's disease maps on chromosome 21. *Science*, 235(4791):885–890, 1987.

[7] Christian Haass and Dennis J. Selkoe. Cellular processing of β-amyloid precursor protein and the genesis of amyloid β-peptide. *Cell*, 75(6):1039 – 1042, 1993.

[8] Robert Vassar, Brian D. Bennett, Safura Babu-Khan, Steve Kahn, Elizabeth A. Mendiaz, Paul Denis, David B. Teplow, Sandra Ross, Patricia Amarante,

Richard Loeloff, Yi Luo, Seth Fisher, Janis Fuller, Steven Edenson, Jackson Lile, Mark A. Jarosinski, Anja Leona Biere, Eileen Curran, Teresa Burgess, Jean-Claude Louis, Frank Collins, James Treanor, Gary Rogers, and Martin Citron. β-secretase cleavage of alzheimer's amyloid precursor protein by the transmembrane aspartic protease bace. *Science*, 286(5440):735–741, 1999.

[9] Flavio Kamenetz, Taisuke Tomita, Helen Hsieh, Guy Seabrook, David Borchelt, Takeshi Iwatsubo, Sangram Sisodia, and Roberto Malinow. App processing and synaptic function. *Neuron*, 37(6):925 – 937, 2003.

[10] Martin Citron, Tilman Oltersdorf, Christian Haass, Lisa McConlogue, Albert Y. Hung, Peter Seubert, Carmen Vigo-Pelfrey, Ivan Lieberburg, and Dennis J. Selkoe. Mutation of the β-amyloid precursor protein in familial alzheimer's disease increases β-protein production. *Nature*, 360(6405):672–674, December 1992.

[11] Stephanie J. Soscia, James E. Kirby, Kevin J. Washicosky, Stephanie M. Tucker, Martin Ingelsson, Bradley Hyman, Mark A. Burton, Lee E. Goldstein, Scott Duong, Rudolph E. Tanzi, and Robert D. Moir. The alzheimer's disease-associated amyloid β-protein is an antimicrobial peptide. *PLoS ONE*, 5(3):e9505, 03 2010.

[12] Efrat Abramov, Iftach Dolev, Hilla Fogel, Giuseppe D Ciccotosto, Eyal Ruff, and Inna Slutsky. Amyloid-β as a positive endogenous regulator of release probability at hippocampal synapses. *Nat Neurosci*, 12(12):1567–1576, December 2009.

[13] Guerrini R. Salvadori S. D'Ursi A.M. Temussi P.A. Picone D. Crescenzi O., Tomaselli S. Solution structure of the alzheimer amyloid beta-peptide (1-42) in an apolar microenvironment. similarity with a virus fusion domain. *Eur. J. Biochem.*, 269:5642–5648, 2002.

[14] Robert Tycko. Solid state nmr studies of amyloid fibril structure. *Annual Reviews of Physical Chemistry*, 62:279–299, 2011.

[15] JP Colletier, A Laganowsky, M Landau, M Zhao, AB Soriaga, L Goldschmidt, D Flot, D Cascio, MR Sawaya, and D Eisenberg. Molecular basis for amyloid-β polymorphism. *Proceedings of the National Academy of Sciences of the United States of America*, 108(5):16938–43, 2011-10-11 00:00:00.0.

[16] David Eisenberg and Mathias Jucker. The amyloid state of proteins in human diseases. *Cell*, 148:1188–1203, 2012.

[17] M. Cecchini, R. Curcio, M. Pappalardo, R. Melki, and A. Caflisch. A molecular dynamics approach to the structural characterization of amyloid aggregation. *Journal of Molecular Biology*, 357(4):1306 – 1321, 2006.

[18] Fu-Feng Liu, Luo Ji, Xiao-Yan Dong, and Yan Sun. Molecular insight into the inhibition effect of trehalose on the nucleation and elongation of amyloid β-peptide oligomers. *The Journal of Physical Chemistry B*, 113(32):11320–11329, 2009. PMID: 19719268.

[19] Angelo Demuro, Ian Parker, and Grace E. Stutzmann. Calcium signaling and amyloid toxicity in alzheimer disease. *Journal of Biological Chemistry*, 285(17):12463–12468, April 2010.

[20] S. Lesné, L. Kotilinek, and K.H. Ashe. Plaque-bearing mice with reduced levels of oligomeric amyloid-β assemblies have intact memory function. *Neuroscience*, 151(3):745 – 749, 2008.

[21] Dominic M. Walsh and Dennis J. Selkoe. Aβ oligomers-a decade of discovery. *Journal of Neurochemistry*, 101(5):1172–1184, 2007.

[22] Woojin Kim and Michael H. Hecht. Sequence determinants of enhanced amyloidogenicity of alzheimer aβ42 peptide relative to aβ40. *Journal of Biological Chemistry*, 280(41):35069–35076, 2005.

[23] Jesse C. Wiley, Mark Hudson, Kevin C. Kanning, Leslyanne C. Schecterson, and Mark Bothwell. Familial alzheimer's disease mutations inhibit γ-secretase-mediated liberation of β-amyloid precursor protein carboxy-terminal fragment. *Journal of Neurochemistry*, 94(5):1189–1201, 2005.

[24] David R. Borchelt, Gopal Thinakaran, Christopher B. Eckman, Michael K. Lee, Frances Davenport, Tamara Ratovitsky, Cristian-Mihail Prada, Grace Kim, Sophia Seekins, Debra Yager, Hilda H. Slunt, Rong Wang, Mary Seeger, Allan I. Levey, Samuel E. Gandy, Neal G. Copeland, Nancy A. Jenkins, Donald L. Price, Steven G. Younkin, and Sangram S. Sisodia. Familial alzheimer's disease - linked presenilin 1 variants elevate aβ1-42/1-40 ratio in vitro and in vivo. *Neuron*, 17(5):1005 – 1013, 1996.

[25] K. E. Wisniewski, H. M. Wisniewski, and G. Y. Wen. Occurrence of neuropathological changes and dementia of alzheimer's disease in down's syndrome. *Annals of Neurology*, 17(3):278–282, 1985.

[26] Rakez Kayed, Yuri Sokolov, Brian Edmonds, Theresa M. McIntire, Saskia C. Milton, James E. Hall, and Charles G. Glabe. Permeabilization of lipid bilayers is a common conformation-dependent activity of soluble amyloid oligomers in protein misfolding diseases. *Journal of Biological Chemistry*, 279(45):46363–46366, 2004.

[27] Florentina Tofoleanu and Nicolae-Viorel Buchete. Molecular interactions of alzheimer's aβ protofilaments with lipid membranes. *Journal of Molecular Biology*, 421(4-5):572 – 586, 2012.

[28] N Arispe, H B Pollard, and E Rojas. Giant multilevel cation channels formed by alzheimer disease amyloid beta-protein aβ p-(1-40) in bilayer membranes. *Proceedings of the National Academy of Sciences*, 90(22):10573–10577, 1993.

[29] Catherine Rovira, Nicolas Arbez, and Jean Mariani. Aβ(25-35) and aβ(1-40) act on different calcium channels in ca1 hippocampal neurons. *Biochemical and Biophysical Research Communications*, 296(5):1317 – 1321, 2002.

[30] Menelas N. Pangalos J. Steven Jacobsen, Peter Reinhart. Current concepts in therapeutic strategies targeting cognitive decline and disease modification in alzheimer's disease. *NeuroRx*, 2(4):612–626, 2005.

[31] V. John L. Mcconlogue G. Basi E. Thorsett D. Schenks S. Sinha, J. Aanderson. Recent advances in the understanding of the processing of app to beta amyloid peptide. *Annals of the New York Academy of Sciences*, 920:206–208, 2000.

[32] Huaibin Cai, Yanshu Wang, Diane McCarthy, Hongjin Wen, David R. Borchelt, Donald L. Price, and Philip C. Wong. Bace1 is the major β-secretase for generation of aβ peptides by neurons. *Nat Neurosci*, 4(3):233–234, March 2001.

[33] Dennis Selkoe and Raphael Kopan. Notch and presenilin: Regulated intramembrane proteolysis links development and degeneration. *Annual Review of Neuroscience*, 26(1):565–597, 2003. PMID: 12730322.

[34] Michael S. Wolfe. Secretase targets for alzheimer's disease:â identification and therapeutic potential. *Journal of Medicinal Chemistry*, 44(13):2039–2060, 2001. PMID: 11405641.

[35] H. F. Dovey, V. John, J. P. Anderson, L. Z. Chen, P. De Saint Andrieu, L. Y. Fang, S. B. Freedman, B. Folmer, E. Goldbach, E. J. Holsztynska, K. L. Hu, K. L. Johnson-Wood, S. L. Kennedy, D. Kholodenko, J. E. Knops, L. H. Latimer, M. Lee, Z. Liao, I. M. Lieberburg, R. N. Motter, L. C. Mutter, J. Nietz, K. P. Quinn, K. L. Sacchi, P. A. Seubert, G. M. Shopp, E. D. Thorsett, J. S. Tung, J. Wu, S. Yang, C. T. Yin, D. B. Schenk, P. C. May, L. D. Altstiel, M. H. Bender, L. N. Boggs, T. C. Britton, J. C. Clemens, D. L. Czilli, D. K. Dieckman-McGinty, J. J. Droste, K. S. Fuson, B. D. Gitter, P. A. Hyslop, E. M. Johnstone, W-Y. Li, S. P. Little, T. E. Mabry, F. D. Miller, B. Ni, J. S. Nissen, W. J. Porter, B. D. Potts, J. K. Reel, D. Stephenson, Y. Su, L. A. Shipley, C. A. Whitesitt, T. Yin, and J. E. Audia. Functional gamma-secretase inhibitors reduce beta-amyloid peptide levels in brain. *Journal of Neurochemistry*, 76(1):173–181, 2001.

[36] Galli C Stefani M Molinari M Paganetti P, Calanca V. β-site specific intrabodies to decrease and prevent generation of alzheimer's aβ peptide. *JJournal of Cell Biology*, 168:863–868, 2005.

[37] Wurtman RJ Growdon JH Nitsch RM, Slack BE. Release of alzheimer amyloid precursor derivatives stimulated by activation of muscarinic acetylcholine receptors. *Science*, 258:304–307, 1992.

[38] Haass C Lichtenthaler SF. Amyloid at the cutting edge: activation of α-secretase prevents amyloidogenesis in an alzheimer disease mouse model. *The Journal of Clinical Investigation*, 113:1384–1387, 2004.

[39] Dale Schenk, Robin Barbour, Whitney Dunn, Grace Gordon, Henry Grajeda, Teresa Guido, Kang Hu, Jiping Huang, Kelly Johnson-Wood, Karen Khan, Dora Kholodenko, Mike Lee, Zhenmei Liao, Ivan Lieberburg, Ruth Motter, Linda Mutter, Ferdie Soriano, George Shopp, Nicki Vasquez, Christopher Vandevert, Shannan Walker, Mark Wogulis, Ted Yednock, Dora Games, and Peter Seubert. Immunization with amyloid-β attenuates alzheimer-disease-like pathology in the pdapp mouse. *Nature*, 400(6740):173–177, July 1999.

[40] Jodi F. Leverone, Edward T. Spooner, Herman K. Lehman, John D. Clements, and Cynthia A. Lemere. Aβ1-15 is less immunogenic than aβ1-40/42 for intranasal immunization of wild-type mice but may be effective for "boosting". *Vaccine*, 21(17â18):2197 – 2206, 2003.

[41] Richard Dodel, Harald Hampel, Candan Depboylu, Suizhen Lin, Feng Gao, Sabine Schock, Steffi Jäckel, Xing Wei, Katharina Buerger, Christine Höft, Bernhard Hemmer, Hans-Jürgen Möller, Martin Farlow, Wolfgang H. Oertel, Norbert Sommer, and Yansheng Du. Human antibodies against amyloid β peptide: A potential treatment for alzheimer's disease. *Annals of Neurology*, 52(2):253–256, 2002.

[42] C Depboylu H Hampel L Frolich A Haag U Hemmeter S Paulsen S Teipel S Brettschneider A Spottke C Nolker H Moller X Wei M Farlow N Sommer R Dodel, Y Du and W Oertel. Intravenous immunoglobulins containing antibodies against β-amyloid for the treatment of alzheimer's disease. *Journal of Neurology, Neurosurgery and Psychiatry*, 75:1472–1474, 2004.

[43] Marcus Fändrich. Oligomeric intermediates in amyloid formation: Structure determination and mechanisms of toxicity. *Journal of Molecular Biology*, 421(4-5):427 – 440, 2012.

[44] Jan Bieschke, Martin Herbst, Thomas Wiglenda, Ralf P Friedrich, Annett Boeddrich, Franziska Schiele, Daniela Kleckers, Juan Miguel Lopez del Amo, Björn A Grüning, Qinwen Wang, Michael R Schmidt, Rudi Lurz, Roger Anwyl, Sigrid Schnoegl, Marcus Fändrich, Ronald F Frank, Bernd Reif, Stefan Günther, Dominic M Walsh, and Erich E Wanker. Small-molecule conversion of toxic oligomers to nontoxic β-sheet-rich amyloid fibrils. *Nat Chem Biol*, 8(1):93–101, January 2012.

[45] Irene H. Cheng, Kimberly Scearce-Levie, Justin Legleiter, Jorge J. Palop, Hilary Gerstein, Nga Bien-Ly, Jukka Puoliväli, Sylvain Lesné, Karen H. Ashe, Paul J. Muchowski, and Lennart Mucke. Accelerating amyloid-β fibrillization reduces oligomer levels and functional deficits in alzheimer disease mouse models. *Journal of Biological Chemistry*, 282(33):23818–23828, 2007.

[46] Mihaela Necula, Rakez Kayed, Saskia Milton, and Charles G. Glabe. Small molecule inhibitors of aggregation indicate that amyloid β oligomerization and

fibrillization pathways are independent and distinct. *Journal of Biological Chemistry*, 282(14):10311–10324, 2007.

[47] Cheryl A. Hawkes, Vivian Ng, and JoAnne McLaurin. Small molecule inhibitors of aβ-aggregation and neurotoxicity. *Drug Development Research*, 70(2):111–124, 2009.

[48] Jermont Chen, Anne H. Armstrong, Angela N. Koehler, and Michael H. Hecht. Small molecule microarrays enable the discovery of compounds that bind the alzheimer's aβ peptide and reduce its cytotoxicity. *Journal of the American Chemical Society*, 132(47):17015–17022, 2010.

[49] Torleif Härd and Christofer Lendel. Inhibition of amyloid formation. *Journal of Molecular Biology*, 421(4-5):441 – 465, 2012.

[50] Ron O. Dror, Morten Ø. Jensen, David W. Borhani, and David E. Shaw. Exploring atomic resolution physiology on a femtosecond to millisecond timescale using molecular dynamics simulations. *The Journal of General Physiology*, 135(6):555–562, 2010.

[51] Ron O. Dror, Robert M. Dirks, J.P. Grossman, Huafeng Xu, and David E. Shaw. Biomolecular simulation: A computational microscope for molecular biology. *Annual Review of Biophysics*, 41(1):429–452, 2012.

[52] Richard A. Friesner and Victor Guallar. Ab initio quantum chemical and mixed quantum mechanics/molecular mechanics (qm/mm) methods for studying enzymatic catalysis. *Annual Review of Physical Chemistry*, 56(1):389–427, 2005. PMID: 15796706.

[53] D van der Spoel, E Lindahl, B Hess, G Groenhof, A E Mark, and H J C Berendsen. Gromacs: Fast, flexible and free. *J. Comp. Chem.*, 26:1701–1718, 2005.

[54] C. Kutzner, D. van der Spoel, M. Fechner, Erik Lindahl, Udo W. Schmitt, Bert L. de Groot, and Helmut Grubmuller. Speeding up parallel gromacs on high-latency networks. *J. Comp. Chem*, 28:2075–2084, 2007.

[55] Berk Hess, Carsten Kutzner, David Van Der Spoel, and Erik Lindahl. Gromacs 4.0: algorithms for highly efficient, load-balanced, and scalable molecular simulation. *J Chem Theory Comput.*, 4:435–447, 2008.

[56] Kresten Lindorff-Larsen, Stefano Piana, Kim Palmo, Paul Maragakis, John L. Klepeis, Ron O. Dror, and David E. Shaw. Improved side-chain torsion potentials for the amber ff99sb protein force field. *Proteins: Structure, Function, and Bioinformatics*, 78(8):1950–1958, 2010.

[57] Phuong H. Nguyen, Mai Suan Li, and Philippe Derreumaux. Effects of all-atom force fields on amyloid oligomerization: replica exchange molecular dynamics simulations of the a[small beta]16-22 dimer and trimer. *Phys. Chem. Chem. Phys.*, 13:9778–9788, 2011.

[58] Kresten Lindorff-Larsen, Paul Maragakis, Stefano Piana, Michael P. Eastwood, Ron O. Dror, and David E. Shaw. Systematic validation of protein force fields against experimental data. *PLoS ONE*, 7(2):e32131, 02 2012.

[59] Berk Hess, Henk Bekker, Herman J. C. Berendsen, and Johannes G. E. M. Fraaije. Lincs: A linear constraint solver for molecular simulations. *Journal of Computational Chemistry*, 18(12):1463–1472, 1997.

[60] J.P. Ryckaert, G. Ciccotti, and H.J.C. Berendsen. Numerical integration of the cartesian equations of motion of a system with constraints: molecular dynamics of n-alkanes. *Journal of Computational Physics*, 23(3):327–341, 1977.

[61] Darrin York Tom Darden and Lee Pedersen. Particle mesh ewald: An n·log(n) method for ewald sums in large systems. *Journal of Chemical Physics*, 98:10089, 1993.

[62] Davide Donadio Giovanni Bussi and Michele Parrinello. Canonical sampling through velocity rescaling. *Journal of Chemical Physics*, 126:014101, 2007.

[63] M. Parrinello and A. Rahman. Polymorphic transitions in single crystals: A new molecular dynamics method. *Journal of Applied Physics*, 52:7182, 1981.

[64] B. Hess A. R. van Buuren E. Apol P. J. Meulenhoff D. P. Tieleman A. L. T. M. Sijbers K. A. Feenstra R. van Drunen D. van der Spoel, E. Lindahl and H. J. C. Berendsen. *Gromacs User Manual version 4.5.4*. www.gromacs.org, 2010.

[65] Schrödinger, LLC. The PyMOL molecular graphics system, version 1.3r1. August 2010.

[66] BL De Groot, DMF Van Aalten, RM Scheek, A. Amadei, G. Vriend, HJC Berendsen, et al. Prediction of protein conformational freedom from distance constraints. *Proteins Structure Function and Genetics*, 29(2):240–251, 1997.

[67] Junmei Wang, Wei Wang, Peter A. Kollman, and David A. Case. Automatic atom type and bond type perception in molecular mechanical calculations. *Journal of Molecular Graphics and Modelling*, 25(2):247 – 260, 2006.

[68] Mahmoud A. A. Ibrahim. Molecular mechanical study of halogen bonding in drug discovery. *Journal of Computational Chemistry*, 32(12):2564–2574, 2011.

[69] Michal Kolar and Pavel Hobza. On extension of the current biomolecular empirical force field for the description of halogen bonds. *Journal of Chemical Theory and Computation*, 8(4):1325–1333, 2012.

[70] Vincent Zoete, Michel A. Cuendet, Aurélien Grosdidier, and Olivier Michielin. Swissparam: A fast force field generation tool for small organic molecules. *Journal of Computational Chemistry*, 32(11):2359–2368, 2011.

[71] Daniel Seeliger, Jürgen Haas, and Bert L. de Groot. Geometry-based sampling of conformational transitions in proteins. *Structure*, 15(11):1482 – 1492, 2007.

[72] Katarina Hart, Nicolas Foloppe, Christopher M. Baker, Elizabeth J. Denning, Lennart Nilsson, and Alexander D. MacKerell. Optimization of the charmm additive force field for dna: Improved treatment of the bi/bii conformational equilibrium. *Journal of Chemical Theory and Computation*, 8(1):348–362, 2012.

[73] Michael W. Mahoney and William L. Jorgensen. A five-site model for liquid water and the reproduction of the density anomaly by rigid, nonpolarizable potential functions. *Journal of Chemical Physics*, 112:8910–8922, 2000.

[74] A Lomakin, D S Chung, G B Benedek, D A Kirschner, and D B Teplow. On the nucleation and growth of amyloid beta-protein fibrils: detection of nuclei and quantitation of rate constants. *Proceedings of the National Academy of Sciences*, 93(3):1125–1129, 1996.

[75] Aleksey Lomakin, David B. Teplow, Daniel A. Kirschner, and George B. Benedek. Kinetic theory of fibrillogenesis of amyloidβ-protein. *Proceedings of the National Academy of Sciences*, 94(15):7942–7947, 1997.

[76] Wolfgang Kabsch and Christian Sander. Dictionary of protein secondary structure: Pattern recognition of hydrogen-bonded and geometrical features. *Biopolymers*, 22(12):2577–2637, 1983.

[77] F Ulrich Hartl and Manajit Hayer-Hartl. Converging concepts of protein folding in vitro and in vivo. *Nat Struct Mol Biol*, 16(6):574–581, June 2009.

Erklärung nach §13(8) der Prüfungsordnung für den Bachelor-Studiengang Physik und den Master-Studiengang Physik an der Universität Göttingen:

Hiermit erkläre ich, dass ich diese Abschlussarbeit selbständig verfasst habe, keine anderen als die angegebenen Quellen und Hilfsmittel benutzt habe und alle Stellen, die wörtlich oder singemäß aus veröffentlichten Schriften entnommen wurden, als solche kenntlich gemacht habe.
Darüberhinaus erkläre ich, dass diese Abschlussarbeit nicht, auch nicht auszugsweise, im Rahmen einer nichtbestandenen Prüfung an dieser oder einer anderen Hochschule eingereicht wurde.

Göttingen, den January 28, 2013

(Julian Tim Brennecke)